European Journal of Mechanics A/Solids 28 (2009) 195–201

Contents lists available at ScienceDirect

European Journal of Mechanics A/Solids

www.elsevier.com/locate/ejmsol

The influence of mechanical constraint upon the switching of a ferroelectric memory capacitor

I. Pane [a,*], N.A. Fleck [b], D.P. Chu [b], J.E. Huber [c]

[a] Department of Civil Engineering, Bandung Institute of Technology, Ganesha 10, Bandung 40132, Indonesia
[b] Department of Engineering, University of Cambridge, Trumpington Street, CB2 1PZ, UK
[c] Department of Engineering Science, University of Oxford, Parks Road, OX1 3PJ, UK

ARTICLE INFO

Article history:
Received 2 May 2008
Accepted 14 September 2008
Available online 20 September 2008

Keywords:
Ferroelectric
Memory
Thin film
Stress
Model

ABSTRACT

The role of mechanical constraint upon the switching response of a ferroelectric thin film memory capacitor is explored. The memory capacitor is represented by a two dimensional ferroelectric island whose non-linear behaviour is modelled by a crystal plasticity constitutive law within the finite element method. The switching response of the device, in terms of remnant charge storage, is determined as a function of geometry and constraint. Various types of constraint on the ferroelectric capacitor are considered, including the presence of a silicon dioxide passivation layer, a silicon substrate and metallic electrodes. The effect of the relative resistance to 90 degree switching and 180 degree switching is also explored in a tetragonal ferroelectric device. Throughout the study, the finite element calculations are compared with the behaviour of a material element subjected to various degrees of mechanical constraint.

1. Introduction

Ferroelectric Random Access Memory (FeRAM) is a candidate non-volatile memory for high speed computers. It is fast for reading and writing, is highly re-writable, scalable, and is compatible with Si technology – either as a stand-alone chip or embedded within an on-chip system. It has a huge market potential for low-power non-volatile memory devices, and is the subject of considerable current research interest (Scott et al., 2005; Bez and Pirovano, 2004). Yet, the successful development of FeRAM is limited by a lack of understanding of its switching response. For instance, the roles of substrate clamping and the constraining effect of the electrode layers and the passivation medium upon FeRAM performance are not well understood.

The cross-section of a typical ferroelectric capacitor is shown in Fig. 1(a). It comprises a ferroelectric film of thickness about 100 nm, sandwiched between electrodes, each of thickness about 100 nm. The device is grown on a silicon substrate and is embedded within a silicon oxide passivation layer. During operation, individual bits of binary data are represented by the local polarisation of the film, with upward and downward polarisation corresponding to the two binary states (see Fig. 1(b)). A sub-nanosecond voltage pulse is used to switch the state, and the ensuing polarisation can be detected by sensing charge or electric field (Chu, 2004).

The successful operation of a FeRAM device relies upon the non-linear switching of polarisation. Since switching involves a change in remnant strain, the substrate and passivation layer constrain switching and induce deleterious stresses. The ongoing reduction of the CMOS feature size (ITRS, 2007) demands a corresponding reduction in the size of the ferroelectric capacitor. Consequently the capacitor must be designed for the maximum possible polarisation switch, to provide a sufficient charge flow for detection of the memory state. Although a substantial research effort has focused on the synthesis and electrical characterisation of FeRAM devices (Aucelio, 2006; Kohlstedt et al., 2005), there is little work on the role of mechanical constraint and its impact on the achievable polarisation. The main aim of the current study is to explore the effect of mechanical constraint by adjacent layers upon the switching response of a ferroelectric capacitor.

In a previous study, Pane et al. (2008) reported the effect of geometry on the performance of thin film ferroelectric capacitors. The devices were assumed to be bonded directly onto a Si substrate and the mechanical effects of the electrodes and passivation layer were neglected. The current paper focuses on the behaviour of ferroelectric devices constrained by realistic surroundings, including electrodes of finite thickness, and a passivation layer. First, the switching response of a material element under various degrees of mechanical constraint is calculated. Second, a mechanically constrained two dimensional ferroelectric island is modelled by the finite element method. The aspect ratio of the ferroelectric island is varied and selected mechanical constraints are applied due to the presence of a SiO_2 passivation layer, a Si substrate and

* Corresponding author.
E-mail address: ivpane@netscape.net (I. Pane).

0997-7538/$ – see front matter
doi:10.1016/j.euromechsol.2008.09.002

metallic electrodes (see Fig. 2). The sensitivity of response to the relative resistance of 90° and 180° switching systems is also explored; in practice, the operation of competing switching systems can be achieved by controlling the composition and doping of the ferroelectric. Our study reveals that the remnant charge is sensitive to the details of device geometry and to the level of imposed constraint.

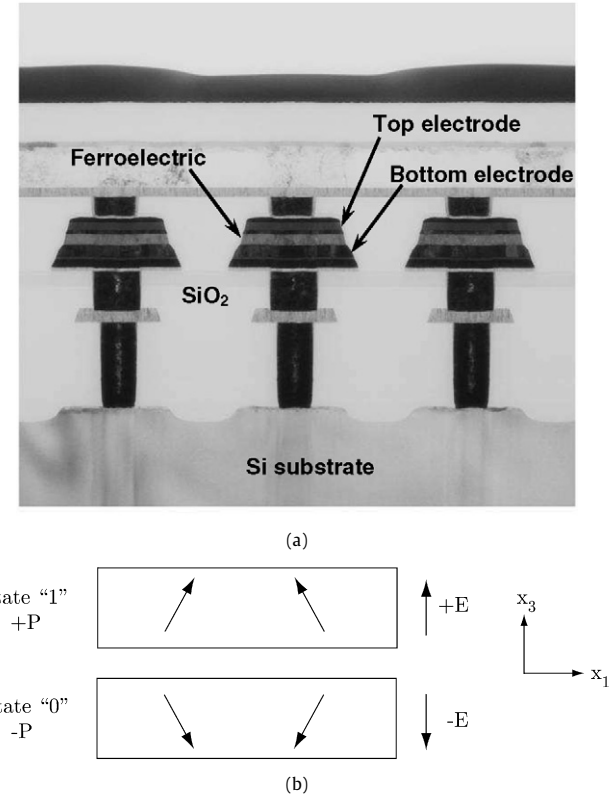

Fig. 1. (a) Cross-sectional TEM image of integrated ferroelectric thin film capacitors (with permission from Seiko-Epson, Japan). (b) The principle of operation of a ferroelectric memory capacitor.

2. Theory and modelling

2.1. Ferroelectric constitutive law

The single crystal switching model of Huber et al. (1999) is employed in a rate dependent formulation, following Huber and Fleck (2001). The total strain ε_{ij} and electric displacement D_i are written as the sum of remnant parts $(\varepsilon^r_{ij}, P_i)$ and reversible parts $(\varepsilon_{kl} - \varepsilon^r_{kl}, D_i - P_i)$. The reversible strain and electric displacement are related to the stress σ_{ij} and electric field E_i by linear piezoelectric relations, so that

$$\sigma_{ij} = c_{ijkl}\left(\varepsilon_{kl} - \varepsilon^r_{kl}\right) - e_{kij}E_k, \tag{1}$$

$$D_i = e_{ikl}\left(\varepsilon_{kl} - \varepsilon^r_{kl}\right) + \kappa^{\varepsilon}_{ik}E_k + P_i, \tag{2}$$

where $e_{kij} = c_{ijmn}d_{kmn}$, $\kappa^{\varepsilon}_{ik} = \kappa^{\sigma}_{ik} - d_{irs}c_{pqrs}d_{kpq}$, κ^{σ}_{ik} is the dielectric permittivity tensor, c_{ijkl} is the elastic stiffness tensor, and d_{kij} is the piezoelectric tensor.

A representative volume of a single tetragonal ferroelectric crystal has $M = 6$ crystal variants or domain types corresponding to the six polarisation directions shown in Fig. 3. Let the Ith domain have volume fraction c_I and polarisation direction n_i. For simplicity, the elastic stiffness c_{ijkl} and dielectric permittivity κ^{σ}_{ik} are taken to be isotropic and do not vary from domain to domain. Then, c_{ijkl} depends only upon the shear modulus μ and Poisson ratio

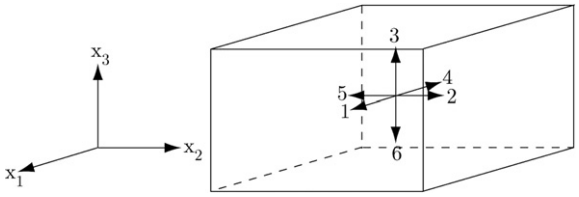

Fig. 3. Polarisation directions in a [100]-oriented tetragonal crystal.

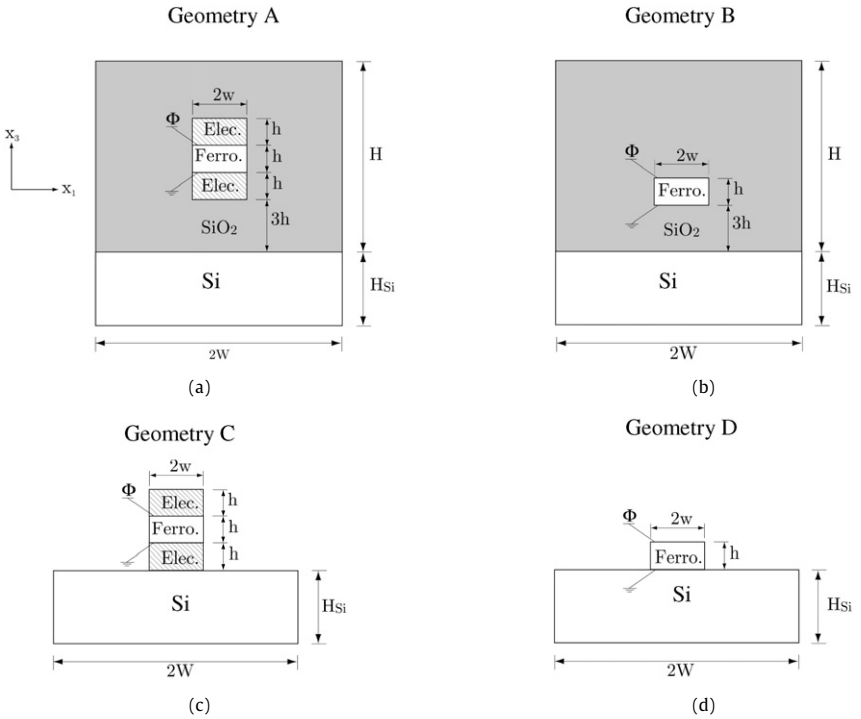

Fig. 2. Four idealised 2D geometries of the ferroelectric device.

ν, while the isotropic permittivity tensor scales with a single parameter κ. The piezoelectric tensor of the Ith domain is given by

$$d^I_{ijk} = d_{33} n_i n_j n_k + d_{31}(n_i \delta_{jk} - n_i n_j n_k) + d_{15}(\delta_{ij} n_k - 2 n_i n_j n_k + \delta_{ik} n_j), \quad (3)$$

where d_{33}, d_{31}, and d_{15} are material coefficients. The remnant strain and polarisation of the Ith domain are respectively $\varepsilon^{r,I}_{ij} = \varepsilon_0(n_i n_j - \delta_{ij})/2$ and $P^I_i = P_0 n_i$, where ε_0 and P_0 are material constants defining the magnitude of remnant strain and polarisation in the domain.

The constitutive model proceeds on the assumption that the stress and electric field are uniform over the representative volume, while the remnant strain and polarisation are given by volume averages. Consequently, the macroscopic piezoelectric tensor, d_{ijk}, equals to $\sum_{I=1}^{M} c_I d^I_{ijk}$. Switching systems (also known as transformation systems) allow for the transformation of one variant type (J) into another type (I). The total number of switching systems that can be active simultaneously in a tetragonal crystal is 15.

Full switching of the αth transformation generates a change of remnant strain by $\Delta\varepsilon^{r,\alpha}_{ij} = \varepsilon^{r,I}_{ij} - \varepsilon^{r,J}_{ij}$, of remnant polarisation by $\Delta P^\alpha_i = P^I_i - P^J_i$, and of the piezoelectric tensor by $\mathbf{\Delta} d^\alpha_{ijk} = d^I_{ijk} - d^J_{ijk}$. Using these quantities, the driving force G^α for the αth transformation, converting variant J to variant I is:

$$G^\alpha = \sigma_{ij}\Delta\varepsilon^{r,\alpha}_{ij} + E_i \Delta P^\alpha_i + \sigma_{ij}\Delta d^\alpha_{ijk} E_k. \quad (4)$$

Huber et al. (1999) and Kessler and Balke (2001) identified G^α as the thermodynamic driving force for domain wall motion.

Let the rate of change of domain volume fraction c_I due to the αth transformation be $\dot{f}^\alpha$. Following Huber and Fleck (2001), a rate dependent formulation can be used to model the switching process, with

$$\dot{f}^\alpha = \dot{f}_0 \left| \frac{G^\alpha}{G^\alpha_c} \right|^{m-1} \frac{G^\alpha}{G^\alpha_c} \left(\frac{c_I}{c_0} \right)^{1/k}. \quad (5)$$

In Eq. (5), $\dot{f}_0$ is a reference switching rate, G^α_c is the critical value of G^α at which there is a rapid increase in transformation rate, and c_0 is the initial volume fraction of crystal variant I. The rate exponents m and k control the rapidity of the onset of switching and the saturation of switching, respectively. The resulting rates of change of remnant strain, remnant polarisation, and of the piezoelectric tensor are given by

$$\dot{\varepsilon}^r_{ij} = \sum_{\alpha=1}^{N} \dot{f}^\alpha \Delta\varepsilon^{r,\alpha}_{ij}, \quad \dot{P}_i = \sum_{\alpha=1}^{N} \dot{f}^\alpha_0 \Delta P^\alpha_i, \quad \dot{d}_{ijk} = \sum_{\alpha=1}^{N} \dot{f}^\alpha \Delta d^\alpha_{ijk}. \quad (6)$$

In the rate independent limit ($m \gg 1$), G^α_c is the energy barrier for the αth transformation. The value of G^α_c for 90° and 180° switching systems can be expressed in terms of the electric field strength required to cause switching in a single crystal. Assume that the crystal has the six possible polarisation directions shown in Fig. 3, and electric field is applied parallel to the x_3 direction. In the rate independent limit, Eqs. (4) and (5) then give $G^{180}_c = 2E_{180}P_0$ for 180° switching and $G^{90}_c = \sqrt{2}E_{90}P_0$ for 90° switching, where E_{180} and E_{90} are the electric fields required for 180° and 90° switching, respectively. We introduce the parameter $\bar{r} = G^{90}_c/(G^{180}_c + G^{90}_c)$ where $0 \leqslant \bar{r} \leqslant 1$ to characterise the propensity for 180° versus 90° switching. When $\bar{r} = 0, 90°$ switching dominates, while $\bar{r} = 1$ corresponds to 180° switching. $\bar{r}$ is varied by changing the value of G^{90}_c while holding $G^{180}_c = 2E_{180}P_0$ constant. The limits $\bar{r} \to 1$ and $\bar{r} \to 0$ are achieved by switching off entirely the 90° or 180° transformations, respectively.

2.2. Finite element model

The constitutive law of Section 2.1 has been implemented in two dimensional finite elements, as detailed by Pane et al. (2008). 6-noded plane strain elements are used, and the rate tangent formulation of Peirce et al. (1983) is employed to stabilise the highly non-linear numerical scheme that results from Eq. (5) (see also Haug et al., 2007; Pathak and McMeeking, 2008). Throughout this study, the ferroelectric solid is represented by a single crystal of tetragonal material with the [100] crystal direction normal to the face of the film and along the x_3-axis of Fig. 1. Calculations are carried out in plane strain ($\varepsilon_{22} = 0$) unless otherwise stated.

We consider two distinct classes of problem: the switching of a two dimensional device in various geometric arrangements as shown in Fig. 2, and the switching of a material element under various degrees of imposed mechanical constraint. The two dimensional (2D) models of the ferroelectric memory capacitor are:

- *Geometry A* (Fig. 2(a)): a ferroelectric island and elastic electrode layers are encapsulated within an elastic SiO_2 passivation layer, and the encapsulation is bonded to a Si substrate. This closely resembles the actual geometry of a FeRAM device.
- *Geometry B* (Fig. 2(b)): a ferroelectric island without electrode layers is encapsulated in an elastic SiO_2 passivation, with an underlying Si substrate; this represents the case where the electrode layers are much thinner than the ferroelectric layer. A comparison with geometry A allows for an examination of the significance of the mechanical constraint against switching imposed by the electrodes.
- *Geometry C* (Fig. 2(c)): an unpassivated ferroelectric island with elastic electrode layers, on a Si substrate; this geometry is typical of a laboratory test structure. This allows for an assessment of the significance of the SiO_2 passivation upon switching, when compared with geometry A.
- *Geometry D* (Fig. 2d): an unpassivated ferroelectric island without electrode layers, but bonded to a Si substrate. This geometry represents an idealised laboratory test structure with electrode layers much thinner than the ferroelectric layer.

For each of the above 2D geometries, the finite element model has a ferroelectric capacitor of thickness h, while the substrate has thickness $H_{Si} = 15h$. The passivation layer, where present, has total thickness $H = 20h$ with the capacitor embedded a distance $3h$ from the substrate, as shown in Fig. 2. These choices represent a thick SiO_2 passivation on a thick Si substrate as is common in practical devices. The ferroelectric capacitor has width $2w$ and the total model width is $2W$, with $W = 10w$ such that the capacitor is remote from the edges of the model. Perfect mechanical bonding at all interfaces is assumed and all layers have isotropic elastic properties, with Young's modulus E and Poisson ratio ν as listed in Table 1. The electrodes, where present, have thickness h and are assumed to be perfectly conducting, resulting in a constant voltage boundary condition on the ferroelectric–electrode interface. For simplicity, the SiO_2 layer and Si substrate are taken to be perfectly insulating, weak dielectrics, so that charge-free boundary conditions exist at the ferroelectric–SiO_2 interface, with zero electric displacement external to the ferroelectric layer. The sides

Table 1
Elastic properties of the layers.

Material	Young's modulus E (GPa)	Poisson ratio ν
PZT ferroelectric	160	0.3
Platinum (Pt) electrodes	160	0.38
SiO_2 passivation	50	0.2
Si substrate	160	0.2

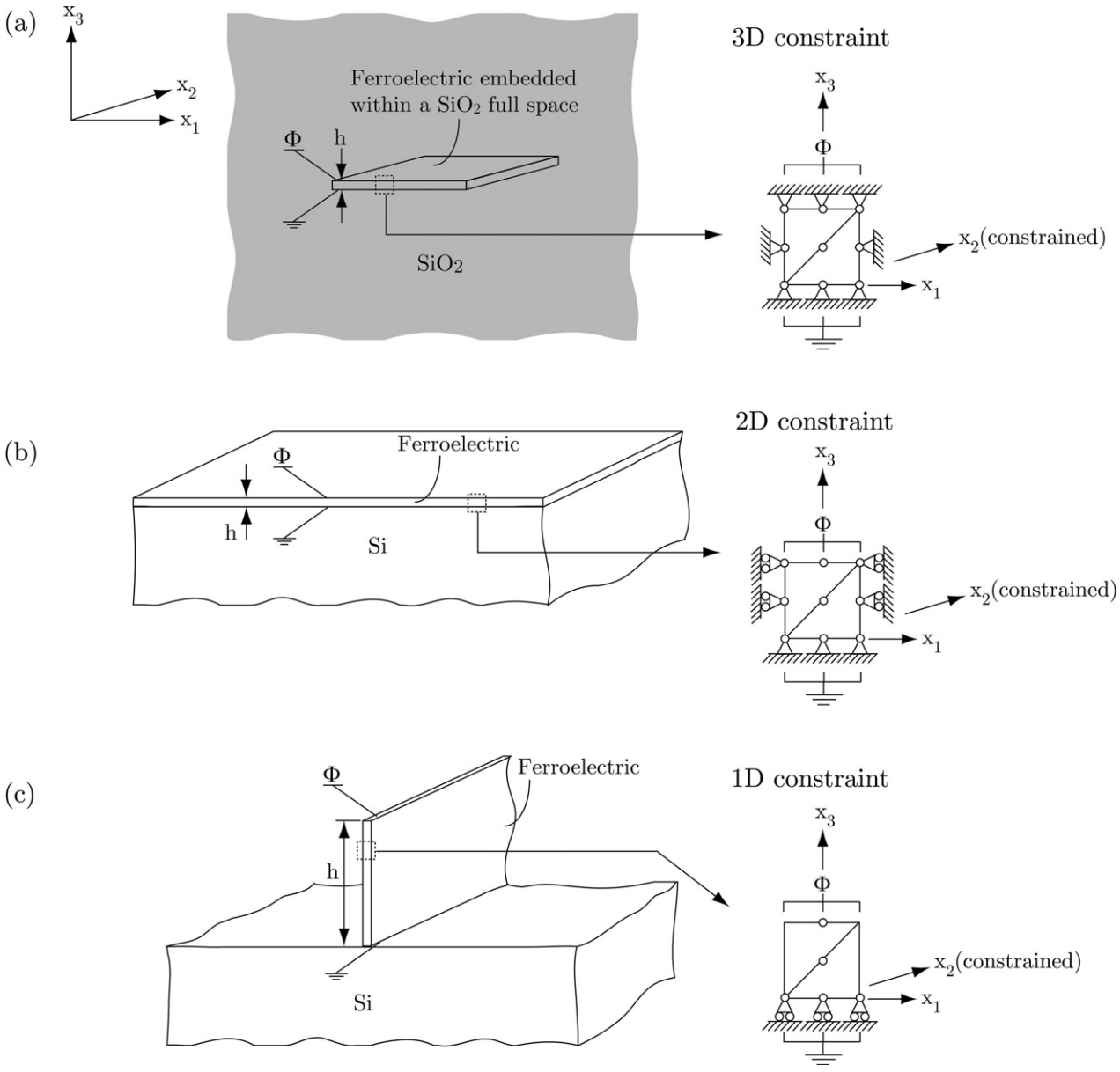

Fig. 4. Constrained thin films, as represented by a material element under various degrees of mechanical constraint.

of the 2D model are taken to be traction and charge free. Model parameters for the ferroelectric layer are chosen to be representative of a soft PZT composition and are given in Table 2; see Huber and Fleck (2004) for a discussion of the fitting of model parameters. The initial conditions in the film, due to processing, may have particular domain structures and a residual stress state. However, in the present study we simplify this initial state by assuming equal volume fractions $c_I = c_0 = 1/6$ of each domain type, and zero residual stress. These assumptions may be justified on the basis that we study the stable hysteresis behaviour after several cycles of saturated switching, so that the influence of the initial state is greatly reduced. Modelling was carried out by applying a uniform, time varying, electrical potential difference $\Phi(t)$ between the top and bottom faces of the ferroelectric capacitor.

Table 2
Material parameters used in the simulations.

Parameter	Value	Unit
Remanent polarisation (P_0)	0.5	$\mathrm{C\,m^{-2}}$
Remanent strain (ε_0)	1%	–
d_{33}	300×10^{-12}	$\mathrm{m\,V^{-1}}$
d_{31}	-135×10^{-12}	$\mathrm{m\,V^{-1}}$
d_{15}	525×10^{-12}	$\mathrm{m\,V^{-1}}$
κ	5.0×10^{-9}	$\mathrm{F\,m^{-1}}$
Creep exponent m	5.0	–
Saturation exponent k	1.0	–
Reference rate $\dot{f}_0$	2.0	$\mathrm{s^{-1}}$
Switching field E_{180}	2.0	$\mathrm{MV\,m^{-1}}$

3. Effect of constraint upon the response of a material element

Before turning to the response of the 2D ferroelectric islands modelled by the finite element method, it is instructive to explore directly the effect of the degree of mechanical constraint upon the switching response of a ferroelectric material element. Recall that the electromechanical state in a 3D device is spatially uniform at material points remote from boundaries and geometric discontinuities. The degree of mechanical constraint experienced by a device

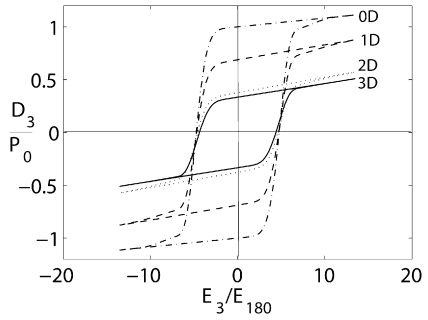

Fig. 5. Hysteresis loops of a ferroelectric layer under 0D, 1D, 2D, and 3D constraints, $\bar{r} = 0.5$.

ranges from fully clamped to unsupported, depending upon the particular geometry. The following idealised cases can be identified:

- *3D constraint* (Fig. 4(a)), representing a fully encapsulated 3D device.
- *2D constraint* (Fig. 4(b)), representing an unpassivated (or passivated) film bonded to a substrate.
- *1D constraint* (Fig. 4(c)). This mimics a free-standing film, but constrained along a single edge to behave in plane-strain.
- *0D constraint*. A material element without mechanical constraint, representing a free-standing film.

The response of a material element under these various degrees of constraint may be calculated directly from the constitutive model, without recourse to the finite element method. However, for computational convenience, we have calculated the response of the material element in each case using a pair of 6-noded elements with imposed boundary conditions as depicted on the right-hand side of Fig. 4. The material properties are listed in Table 2. Initially, each domain has an equal volume fraction of 1/6 and the material element is stress-free. Then, 2.5 cycles of triangular waveform $\Phi(t)$ are applied, with a frequency of $5000\hat{f}_0$ and amplitude about $3h$ times the effective coercive field (note that this differs significantly from E_{180} because of the high frequency of loading). Numerical experiments reveal that stable electric displacement D versus electric field E hysteresis loops are obtained after only a few cycles. Stable hysteresis loops corresponding to the material element subject to constraints 0D through to 3D constraints are shown in Fig. 5, with the material parameter $\bar{r}$ set at 0.5 to allow both 90° and 180° switching.

Full switching occurs in the absence of mechanical constraint (0D simulation), and the polarisation then attains a value of $\pm P_0$. With plane strain conditions imposed along the x_2 direction only (1D constraint), negligible switching occurs for the crystal variants 2 and 5 (see Fig. 3) that are polarised in the x_2 direction. Since these variants account for 1/3 of the volume fraction, the resulting remnant polarisation is about $2P_0/3$. Imposition of 2D or 3D constraint severely impedes 90° switching and the remnant polarisation drops to about $P_0/3$.

4. Effect of constraint upon the response of a finite island

Now consider the finite 2D ferroelectric islands of Fig. 2. We can expect their behaviour to be somewhat similar to the constrained material elements discussed in Section 3. However, the degree of mechanical constraint to which they are subjected depends upon their geometry, or aspect ratio. A geometry parameter $\bar{w} = w/(w+h)$ is introduced, such that $0 \leqslant \bar{w} \leqslant 1$. The limit $\bar{w} = 0$ represents a device with height much greater than its width, such as that shown in Fig. 4(c). In contrast, a device with $\bar{w} = 1$ has width much greater than its thickness, as in Fig. 4(b).

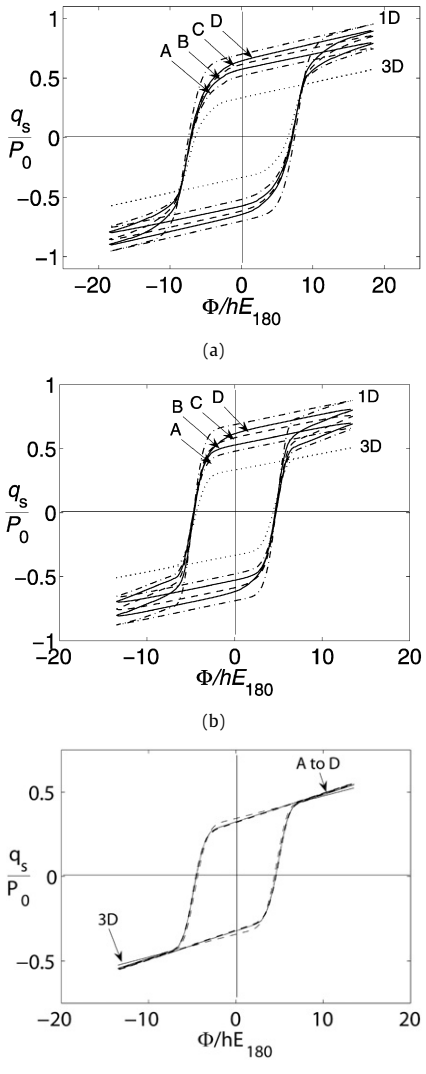

Fig. 6. Hysteresis loops of geometries A to D, for $\bar{w} = 0.5$. The responses of material elements under 1D and 3D constraint are included. (a) In all cases $\bar{r} = 0$. (b) In all cases $\bar{r} = 0.5$. (c) In all cases $\bar{r} = 1$. The remnant charge density q_S under 0D, 1D and 2D constraint is $1.0P_0$, $0.68P_0$ and $0.37P_0$, respectively.

4.1. Remnant charge response of finite 2D island geometries

Saturated polarisation hysteresis loops for geometries A–D and various values of $\bar{r}$ and $\bar{w}$ are given in Fig. 6. Since the electric field and electric displacement are non-uniform in these geometries, the normalised mean electric displacement q_s/P_0 is shown versus normalised mean electric field Φ/hE_{180}, where q_s is the mean charge density on the top electrode-ferroelectric interface. The saturated hysteresis loops of Fig. 6 reveal the sensitivity of performance of the finite 2D island to the various mechanical constraints imposed by the electrodes, encapsulation and substrate. Results are shown in Fig. 6(a)–(c) for the choice $\bar{r} = 0$ (90° switching), 0.5 (mixed switching) and 1 (180° switching), respectively. Recall that 90° switching is accompanied by a change in strain, whereas 180° switching does not induce a change in strain. Consequently, there is a diminishing effect of mechanical constraint upon the switching response as $\bar{r}$ is increased. It is clear from Fig. 6(c) that when $\bar{r} = 1$, the four finite geometries have an almost identical response to that of a material element under 3D constraint. For $\bar{r} < 1$, the remnant charge density q_S decreases as the amount of constraint increases through the sequence of geometries D to A, see Figs. 6(a) and 6(b); in each of these cases the response of the

finite island is intermediate between that for a material element under 1D constraint and under 3D constraint.

There is a fundamental difference in the nature of the constraint imposed by an infinite substrate upon a finite island and upon a thin film. For the thin film, the substrate imposes full in-plane constraint regardless of the relative moduli of film and substrate. In contrast, the degree of constraint upon an island depends upon the ratio of moduli of island to substrate. Full constraint is not achievable for the island. Thus, the hysteresis loops of geometries A to D each display a greater remnant charge than that of a material element under 3D constraint.

The effect of SiO_2 passivation can be seen by comparing the hysteresis loops of geometries A and C (electrode layers present), or of geometries B and D (electrode layer absent). Similarly, the effect of electrode layers can be seen by comparing the hysteresis loops of models A and B for a capacitor with SiO_2 passivation, or by comparing the hysteresis loops of models C and D for a capacitor without passivation. For the choices $\bar{r} = 0$ and 0.5, it is clear that the constraint provided by the passivation layer is enhanced by the presence of the electrodes.

4.2. Sensitivity of response to $\bar{w}$

The remnant charge density q_S is plotted as a function of $\bar{w}$ for $\bar{r} = 0$ and 0.5 in Figs. 7(a) and 7(b), respectively. For $\bar{r} < 1$, there is a monotonic drop in q_S with increasing $\bar{w}$ for geometries C and D (passivation layer absent), whereas q_S first increases and then decreases with increasing $\bar{w}$ for geometries A and B (passivation layer present).

This behaviour can be understood by first considering the limits of $\bar{w} \to 0$ (i.e. $w \to 0$) and $\bar{w} \to 1$ (i.e. $h \to 0$). The geometries A and B are constrained along the x_3 direction by the encapsulation whereas geometries C and D are unconstrained in this direction. Consequently, at both limits $\bar{w} \to 0$ and $\bar{w} \to 1$ the geometries A and B behave like the fully constrained material element of Fig. 4(a). At intermediate values of $\bar{w}$, the level of constraint upon geometries A and B is reduced and consequently q_S is greater than that of the material element under 3D constraint. We note from in Figs. 7(a) and 7(b) that q_S has a peak value at $\bar{w} \approx 0.4$ for geometries A and B. In contrast, the geometries C and D behave like a material element under 1D constraint as $\bar{w} \to 0$, and under 2D constraint as $\bar{w} \to 1$. The mechanical constraint upon geometries C and D is always less than that upon A and B, and consequently their q_S values exceed those of geometries A and B for any given value of $\bar{w}$.

It is interesting to note that the remnant charge responses in Figs. 7(a) and 7(b) are almost identical, suggesting that a variation of $\bar{r}$ between 0 and 0.5 has little effect upon the saturated polarisation. This observation can be explained by considering that 180° switching can manifest itself as two successive 90° transformations. Thus, even when 180° transformations are suppressed, an equivalent transformation process still exists. Next consider the limiting case of $\bar{r} = 1$. Then, surface charge density q_S is due to 180° switching only and there is no effect of mechanical constraint upon the response. In this case, the remnant charge density has the value $q_S = P_0/3$ for all geometries, over the full range of $\bar{w}$.

4.3. Sensitivity of the finite island and constrained material element to $\bar{r}$

It is instructive to plot in Fig. 8 the dependence of q_S upon $\bar{r}$ for the finite island geometries with $\bar{w} = 0.5$, and to compare the behaviours to those of the constrained material elements. q_S decreases monotonically with increasing $\bar{r}$ in all cases. Consistent with the results already shown in Fig. 7, the presence of 90° switching confers sensitivity of q_S to the degree of constraint. 180° switching dominates for $\bar{r}$ above about 0.7 and the responses for the various geometries then converge to a common value.

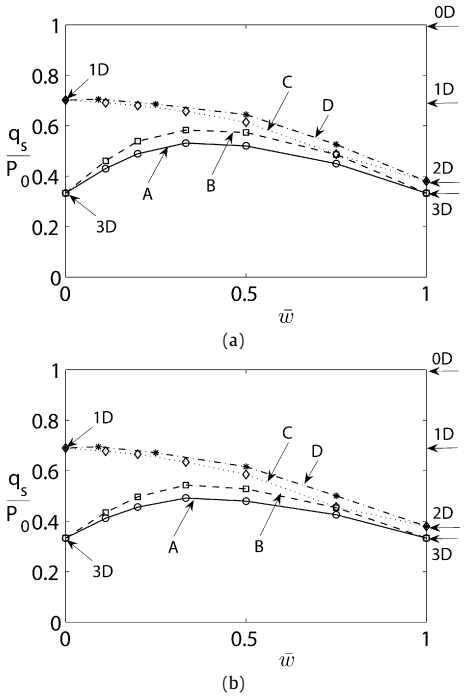

Fig. 7. Sensitivity of remnant charge density to $\bar{w}$ for geometries A to D. Predictions are included for a material element under 0D and 3D constraint. (a) In all cases, $\bar{r} = 0$. (b) In all cases, $\bar{r} = 0.5$.

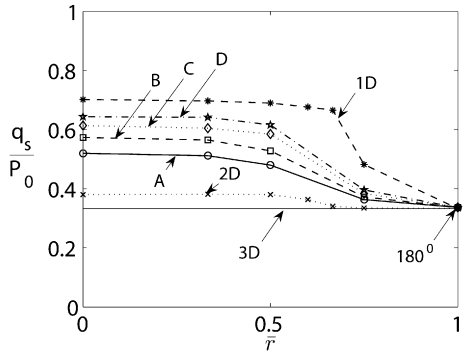

Fig. 8. Sensitivity of remnant charge density to $\bar{r}$ for geometries A to D with $\bar{w} = 0.5$. Predictions for material elements under various degrees of mechanical constraint are included.

5. Concluding comments

A study of the switching behaviour of finite ferroelectric islands with mechanical constraint provides useful qualitative insight into the performance of ferroelectric memory devices. Constraint upon 90° switching arises from a number of device features: the electrodes, encapsulation and the substrate. The relative significance of each of these has been assessed by comparing the responses of the device geometries shown in Fig. 2. The sensitivity of switching response to mechanical constraint is a strong function of the relative resistance to 90° and 180° switching. When 90° switching is more difficult than 180° switching, mechanical constraint becomes less significant. In the limit of purely 180° switching, the response is almost independent of constraint and device geometry. Insight is gained by considering a material element under various degrees of constraint: the response of the material element provides limits on that of the ferroelectric island, and matches

that of the island exactly in certain limiting geometries. From the standpoint of device design, it is shown that an embedded ferroelectric capacitor may exhibit a markedly different response from that of an unpassivated film as commonly used in laboratory test specimens. The study also indicates that an optimal geometry of ferroelectric device exists that maximises the achievable polarisation.

Acknowledgement

This work is supported under EPSRC grant GR/S98412/01.

References

Aucelio, O., 2006. Science and technology of thin films and interfacial layers in ferroelectric and high-dielectric constant heterostructures and application to devices. J. Appl. Phys. 100. Art. 051614.

Bez, R., Pirovano, A., 2004. Non-volatile memory technologies: emerging concepts and new materials. Materials Science in Semiconductor Processing 7, 349–355.

Chu, D.P., 2004. A novel ferroelectric FET based memory cell of minimum size and non-destructive reading. Integrated Ferroelectrics 61, 71–76.

Haug, A., Huber, J.E., Onck, P.R., Van der Giessen, E., 2007. Multi-grain analysis versus self-consistent estimates of ferroelectric polycrystals. J. Mech. Phys. Solids 55 (3), 648–665.

Huber, J.E., Fleck, N.A., 2001. Multi-axial electrical switching of a ferroelectric: theory versus experiment. J. Mech. Phys. Solids 49, 785–811.

Huber, J.E., Fleck, N.A., 2004. Ferroelectric switching: a micromechanics model versus measured behaviour. Eur. J. Mech. A/Solids 23, 203–217.

Huber, J.E., Fleck, N.A., Landis, C.M., McMeeking, R.M., 1999. A constitutive model for ferroelectric polycrystals. J. Mech. Phys. Solids 47, 1663–1697.

ITRS, International Technology Roadmap for Semiconductors, 2007.

Kessler, H., Balke, H., 2001. On the local and average energy release in polarization switching phenomena. J. Mech Phys. Solids 49, 953–978.

Kohlstedt, H., Mustafa, Y., Gerber, A., Petraru, A., Fitsilis, M., Meyer, R., Bottger, U., Waser, R., 2005. Current status and challenges of ferroelectric memory devices. Microelectronic Engineering 80, 296–304.

Pane, I., Fleck, N.A., Huber, J.E., Chu, D.P., 2008. Effect of geometry upon the performance of a thin film memory capacitor. Int. J. Solids Struct. 45, 2024–2041.

Pathak, A., McMeeking, R.M., 2008. Three-dimensional finite element simulations of ferroelectric polycrystals under electrical and mechanical loading. J. Mech. Phys. Solids 56, 663–683.

Peirce, D., Asaro, R.J., Needleman, A., 1983. Material rate dependence and localized deformation in crystalline solids. Acta Metallurgica 31 (12), 1951–1976.

Scott, J.F., Morrison, F.D., Miyake, M., Zubko, P., Lou, X.J., Kugler, V.M., Rios, S., Zhang, M., Tatsuta, T., Tsuji, O., Leedham, T.J., 2005. Recent materials characterizations of 2D and 3D thin film ferroelectric structures. J. Am. Cer. Soc. 88 (7), 1691–1701.